

Construction of explicit symplectic integrators in general relativity. II. Reissner-Nordström black holes

Ying Wang^{1,2}, Wei Sun¹, Fuyao Liu¹, Xin Wu^{1,2,3,†}

1. *School of Mathematics, Physics and Statistics, Shanghai University of Engineering Science, Shanghai 201620, China*

2. *Center of Application and Research of Computational Physics, Shanghai University of Engineering Science, Shanghai 201620, China*

3. *Guangxi Key Laboratory for Relativistic Astrophysics, Guangxi University, Nanning 530004, China*

Emails: wangying424524@163.com (Y. W.), sunweiy@163.com (W. S.), liufuyao2017@163.com (F. L.); † Corresponding Author: wuxin_1134@sina.com (X. W.)

ABSTRACT

In a previous paper, second- and fourth-order explicit symplectic integrators were designed for a Hamiltonian of the Schwarzschild black hole. Following this work, we continue to trace the possibility of the construction of explicit symplectic integrators for a Hamiltonian of charged particles moving around a Reissner-Nordström black hole with an external magnetic field. Such explicit symplectic methods are still available when the Hamiltonian is separated into five independently integrable parts with analytical solutions as explicit functions of proper time. Numerical tests show that the proposed algorithms share the desirable properties in their long-term stability, precision and efficiency for appropriate choices of step sizes. For the applicability of one of the new algorithms, the effects of the black hole's charge, the Coulomb part of the electromagnetic potential and the magnetic parameter on the dynamical behavior are surveyed. Under some circumstances, the extent of chaos gets strong with an increase of the magnetic parameter from a global phase-space structure. No the variation of the black hole's charge but the variation of the Coulomb part is considerably sensitive to affect the regular and chaotic dynamics of particles' orbits. A positive Coulomb part is easier to induce chaos than a negative one.

Unified Astronomy Thesaurus concepts: Black hole physics (159); Computational methods (1965); Computational astronomy (293); Celestial mechanics (211)

1. Introduction

Based on Einstein's theory of general relativity, black holes are a group of solutions of the Einstein's field equations. Usually, black holes have singularities covered by event horizon surfaces. The first black hole's solution for the description of a static and spherically symmetric gravitational field around a point-like mass was given by Schwarzschild (1916). When the mass source in the origin is charged, the Reissner-Nordström (RN) metric (Reissner 1916) became available. A rigorous solution representing the gravitational

field around a rotating central mass is the Kerr metric (Kerr 1963). On the other hand, evidence from observations demonstrated the existence of supermassive black holes with masses from millions to tens of billions of solar masses in centers of nearly all galaxies. In terms of images of M87, a central Kerr black hole is estimated to have mass $M = (6.5 \pm 0.7) \times 10^9 M_\odot$ (M_\odot being the Sun's mass), which is consistent with the result predicted by the general theory of relativity (EHT Collaboration et al. 2019a, b, c). Successful gravitational-wave measurements (Abbott et al. 2016) also provided powerful evidence for the presence of black holes.

Although the relativistic spacetimes like the RN or Kerr metric are highly nonlinear, they are integrable and have analytical solutions because of

the presence of enough constants of motion. The solutions have only formal expressions in terms of quadratures, but cannot be expressed as elementary functions or explicit functions of time. To know detailed information on the solutions how to evolve with time, one had better employ a numerical integration technique to solve the integrable problems. If the central bodies are suffered from perturbations, such as external magnetic fields, the spacetimes become non-integrable in most cases. Under some circumstances, chaos occurs (Takahashi & Koyama 2009; Kopáček et al. 2010; Kopáček & Karas 2014; Stuchlík & Kološ 2016; Pánis et al. 2019; Li & Wu 2019; Stuchlík et al. 2020; Yi & Wu 2020). This chaoticity indicates that a dynamical system is exponentially sensitive dependence on initial conditions (Lichtenberg & Leiberman 1983). In this case, the numerical technique is more indispensable to study the non-integrable systems.

Reliable results from numerical integrators with a good behavior are required, especially in the case of long-term integration of chaotic orbits. The most appropriate solvers are geometric or structure preserving algorithms (Hairer et al. 1999; Seyrich & Lukes-Gerakopoulos 2012; Bacchini et al. 2018a, 2018b; Hu et al. 2019), such as symplectic methods for Hamiltonian systems (Ruth 1983; Wisdom & Holman 1991). They have several advantages over standard explicit integrators, such as the family of explicit Runge-Kutta solvers. The integrals of motion (e.g., energy integral) along the trajectory are nearly conserved for the structure preserving integrators, but their errors increase linearly with time for the standard integration schemes. In addition, the overall phase error only grows linearly with time for the former algorithms, whereas it is normally proportional to the square of the length of the integration interval for the latter schemes (Deng et al. 2020). The above-mentioned curved spacetimes can be expressed in terms of Hamiltonian systems, and thus symplectic integrators are naturally chosen. Standard explicit symplectic integrators, such as a second-order Verlet integrator (Swope et al. 1982), become useless. However, completely implicit symplectic methods (Kopáček et al. 2010; Seyrich & Lukes-Gerakopoulos 2012; Tsang et al. 2015), such as the implicit midpoint scheme (Feng 1986; Brown 2006), or implicit and

explicit combined symplectic methods (Liao 1997; Preto & Saha 2009; Lubich et al. 2010; Zhong et al. 2010; Mei et al. 2013a, 2013b) are used. This is because the Hamiltonians have no separable forms of variables or can be split into two integrable parts without analytical solutions as explicit functions of time. Unfortunately, such implicit integrators are more computationally demanding at the expense of computational time than the same order standard explicit methods. Extended phase-space methods (Pihajoki 2015; Liu et al. 2016; Luo et al. 2017; Li & Wu 2017) are explicit and have good long-term stable behavior in energy errors, but are not symplectic. In a previous work (Wang et al. 2021), we overcame the difficulty in the construction of explicit symplectic integrators for the Schwarzschild metric. In our construction, the Hamiltonian for the Schwarzschild spacetime can be separated into four integrable parts with analytical solutions as explicit functions of proper time. Then, these explicit solvable operators symmetrically composed second- and fourth-order explicit symplectic integrators.

Following the previous work (Wang et al. 2021), we design explicit symplectic integrators for the RN black hole immersed into an external magnetic field. This is one of the main aims in the present paper. Another aim is to know how an increase of the black hole’s charge, the Coulomb parameter of the electromagnetic potential or the magnetic parameter exerts an influence on the dynamical transition of orbits of charged particles around the RN black hole. For the sake of these purposes, we introduce a dynamical model of charged particles moving around the RN black hole surrounded with an external magnetic field in Section 2. Second- and fourth-order explicit symplectic integrators are designed for the magnetized RN spacetime in Section 3. In Section 4, we evaluate the numerical performance of the proposed algorithms, and apply a new integrator to address the question of how the related parameters affect the orbital dynamics of order and chaos. Finally, the main results are concluded in Section 5.

2. Reissner-Nordström black holes

The Schwarzschild black hole with charge Q is the RN black hole. In dimensionless spherical-like coordinates (t, r, θ, ϕ) , the RN spacetime (Reissner

1916) takes the following metric

$$\begin{aligned}
-\tau^2 &= ds^2 = g_{\alpha\beta} dx^\alpha dx^\beta \\
&= -\left(1 - \frac{2}{r} + \frac{Q^2}{r^2}\right) dt^2 + \left(1 - \frac{2}{r} + \frac{Q^2}{r^2}\right)^{-1} dr^2 \\
&\quad + r^2 d\theta^2 + r^2 \sin^2 \theta d\phi^2.
\end{aligned} \tag{1}$$

The speed of light c and the constant of gravity G use geometrized units, $c = G = 1$. M is the mass of black hole, and also takes one unit, $M = 1$. Proper time τ , coordinate time t , radial separation r and charge Q are dimensionless. In practice, the dimensionless operations are obtained via scale transformations: $\tau \rightarrow M\tau$, $t \rightarrow Mt$, $r \rightarrow Mr$ and $Q \rightarrow MQ$. When $|Q| < 1$, this spacetime corresponds to black holes with two event horizons $r_{\pm} = 1 \pm \sqrt{1 - Q^2}$. The spacetime is still a black hole with an event horizon $r = 1$ for $Q = \pm 1$. It has no event horizon but has naked singularities if $|Q| > 1$. Hereafter, the case of black holes with $|Q| \leq 1$ is considered.

The motion of a test particle around the black hole is described by the Lagrangian system

$$\ell = \frac{1}{2} \left(\frac{ds}{d\tau}\right)^2 = \frac{1}{2} g_{\mu\nu} \dot{x}^\mu \dot{x}^\nu, \tag{2}$$

where $\dot{x}^\mu = \mathbf{U}$ is a four-velocity satisfying the relation

$$\mathbf{U} \cdot \mathbf{U} = U^\alpha U_\alpha = g_{\mu\nu} \dot{x}^\mu \dot{x}^\nu = -1. \tag{3}$$

A covariant generalized momentum \mathbf{p} is defined as

$$p_\mu = \frac{\partial \ell}{\partial \dot{x}^\mu} = g_{\mu\nu} \dot{x}^\nu. \tag{4}$$

Because t and ϕ do not explicitly appear in the Lagrangian, there are two constant momentum components

$$p_t = -\left(1 - \frac{2}{r} + \frac{Q^2}{r^2}\right) \dot{t} = -\mathcal{E}, \tag{5}$$

$$p_\phi = r^2 \sin^2 \theta \dot{\phi} = \mathcal{L}. \tag{6}$$

\mathcal{E} and \mathcal{L} denote the particle's energy and angular momentum, respectively.

The Lagrangian corresponds to the Hamiltonian

$$\begin{aligned}
H &= \mathbf{U} \cdot \mathbf{p} - \ell = \frac{1}{2} g^{\mu\nu} p_\mu p_\nu \\
&= -\frac{\mathcal{E}^2}{2} \left(1 - \frac{2}{r} + \frac{Q^2}{r^2}\right)^{-1} + \frac{p_r^2}{2} \left(1 - \frac{2}{r} + \frac{Q^2}{r^2}\right) \\
&\quad + \frac{1}{2} \frac{p_\theta^2}{r^2} + \frac{1}{2} \frac{\mathcal{L}^2}{r^2 \sin^2 \theta}.
\end{aligned} \tag{7}$$

Because of the four-velocity relation (3), this Hamiltonian is always identical to $-1/2$,

$$H = -\frac{1}{2}. \tag{8}$$

By separating the variables in the Hamilton-Jacobi equation, one can find a second integral excluding the two integrals \mathcal{E} and \mathcal{L} in the Hamiltonian system (Carter 1968). Thus, this system is integrable and has formally analytical solutions.

Now, suppose the black hole surrounded by an external magnetic field whose four-vector potential has two nonzero covariant components

$$A_t = -\frac{Q}{r}, \quad A_\phi = \frac{B}{2} g_{\phi\phi} = \frac{B}{2} r^2 \sin^2 \theta, \tag{9}$$

where A_t represents the Coulomb part of the electromagnetic potential (Kopacek & Karas 2014), and B is the strength of the magnetic field parallel to the z axis (Felice & Sorge 2003). The motion of a particle with charge q under the interactions of the black hole's gravity and electromagnetic force is described by the Hamiltonian

$$\begin{aligned}
K &= \frac{1}{2} g^{\mu\nu} (p_\mu - qA_\mu)(p_\nu - qA_\nu) \\
&= -\frac{1}{2} \left(1 - \frac{2}{r} + \frac{Q^2}{r^2}\right)^{-1} \left(E - \frac{Q^*}{r}\right)^2 \\
&\quad + \frac{1}{2} \left(1 - \frac{2}{r} + \frac{Q^2}{r^2}\right) p_r^2 + \frac{1}{2} \frac{p_\theta^2}{r^2} \\
&\quad + \frac{1}{2r^2 \sin^2 \theta} \left(L - \frac{1}{2} \beta r^2 \sin^2 \theta\right)^2,
\end{aligned} \tag{10}$$

where $Q^* = qQ$ is a Coulomb parameter of the electromagnetic potential, and $\beta = qB$. To make the system (10) be dimensionless, we take $K \rightarrow m^2 K$, $E \rightarrow mE$, $p_r \rightarrow mp_r$, $p_\theta \rightarrow mMp_\theta$, $L \rightarrow mML$, $q \rightarrow mq$ and $B \rightarrow B/M$, where m is the particle's mass. The expressions of energy E and angular momentum L of the charged particle become

$$E = \left(1 - \frac{2}{r} + \frac{Q^2}{r^2}\right) \dot{t} + \frac{Q^*}{r}, \tag{11}$$

$$L = r^2 \sin^2 \theta \dot{\phi} + \frac{1}{2} \beta r^2 \sin^2 \theta. \tag{12}$$

Similar to H , K always satisfies the constraint

$$K = -\frac{1}{2}. \tag{13}$$

However, K unlike H has no second integral. Thus, it is non-integrable and has no formally analytical solutions. In this case, a numerical integration method is a convenient tool to work out such a non-integrable system.

3. Construction of explicit symplectic integrators

In view of a symplectic integrator with good geometric and physical properties, it is naturally a prior choice of numerical integrator for the description of long-term qualitative evolution of the Hamiltonian system (7). An explicit symplectic method becomes useless without doubt if this Hamiltonian is separated into two analytically solvable parts. This is because not all analytical solutions of the two splitting parts are explicit functions of proper time τ . An explicit symplectic algorithm fails to be built if the Hamiltonian is split into four analytically integrable parts, as the Hamiltonian of Schwarzschild black hole is in our previous paper (Wang et al. 2021). Thus, it may be necessary that more analytically integrable splitting parts should be given to the Hamiltonian for the construction of explicit symplectic schemes.

Let the Hamiltonian of RN black hole be separated into five separable parts

$$H = H_1 + H_2 + H_3 + H_4 + H_5, \quad (14)$$

where the five sub-Hamiltonians are written as follows:

$$H_1 = \frac{1}{2} \frac{\mathcal{L}^2}{r^2 \sin^2 \theta} - \frac{\mathcal{E}^2}{2} \left(1 - \frac{2}{r} + \frac{Q^2}{r^2}\right)^{-1}, \quad (15)$$

$$H_2 = \frac{1}{2} p_r^2, \quad (16)$$

$$H_3 = -\frac{1}{r} p_r^2, \quad (17)$$

$$H_4 = \frac{p_\theta^2}{2r^2}, \quad (18)$$

$$H_5 = \frac{1}{2} \frac{Q^2}{r^2} p_r^2. \quad (19)$$

H_2 , H_3 and H_4 are the same as those in the Hamiltonian splitting of Schwarzschild black hole in the previous work (Wang et al. 2021).

H_1 has its canonical equations $\dot{r} = \dot{\theta} = 0$ and

$$\begin{aligned} \frac{dp_r}{d\tau} &= -\frac{\partial H_1}{\partial r} = \frac{\mathcal{L}^2}{r^3 \sin^2 \theta} - \frac{\mathcal{E}^2}{r^2} \left(1 - \frac{Q^2}{r}\right) \\ &\quad \cdot \left(1 - \frac{2}{r} + \frac{Q^2}{r^2}\right)^{-2} = \mathfrak{R}(r, \theta), \end{aligned} \quad (20)$$

$$\frac{dp_\theta}{d\tau} = -\frac{\partial H_1}{\partial \theta} = \frac{\mathcal{L}^2 \cos \theta}{r^2 \sin^3 \theta} = \Theta(r, \theta). \quad (21)$$

If \mathcal{A} is taken as a differential operator

$$\mathcal{A} = \mathfrak{R} \frac{\partial}{\partial p_r} + \Theta \frac{\partial}{\partial p_\theta}, \quad (22)$$

then $\mathcal{A}p_r = \dot{p}_r = \mathfrak{R}$ and $\mathcal{A}p_\theta = \dot{p}_\theta = \Theta$. Because r and θ are constants, p_r and p_θ are easily solved. From proper time τ_0 over a proper time step h to proper time $\tau = \tau_0 + h$, the solutions are expressed as

$$p_r = p_{r0} + h\mathfrak{R}(r_0, \theta_0), \quad (23)$$

$$p_\theta = p_{\theta 0} + h\Theta(r_0, \theta_0), \quad (24)$$

where $\mathbf{z}(0) = (r_0, \theta_0, p_{r0}, p_{\theta 0})$ are the solutions at the beginning of the step of length h . We use an exponential operator $e^{h\mathcal{A}}$ to represent the analytical solutions (23) and (24), i.e., $(p_r, p_\theta) = e^{h\mathcal{A}}\mathbf{z}(0)$.

Set \mathcal{B} , \mathcal{C} , \mathcal{D} and \mathcal{F} as differential operators of H_2 , H_3 , H_4 and H_5 , respectively. They are of the following expressions

$$\mathcal{B} = p_r \frac{\partial}{\partial r}, \quad (25)$$

$$\mathcal{C} = -\frac{2}{r} p_r \frac{\partial}{\partial r} - \frac{p_r^2}{r^2} \frac{\partial}{\partial p_r}, \quad (26)$$

$$\mathcal{D} = \frac{p_\theta}{r^2} \frac{\partial}{\partial \theta} + \frac{p_\theta^2}{r^3} \frac{\partial}{\partial p_r}, \quad (27)$$

$$\mathcal{F} = \frac{Q^2}{r^2} p_r \frac{\partial}{\partial r} + Q^2 \frac{p_r^2}{r^3} \frac{\partial}{\partial p_r}. \quad (28)$$

The four sub-Hamiltonians have their analytical solutions

$$e^{h\mathcal{B}} : r = r_0 + hp_{r0}; \quad (29)$$

$$e^{h\mathcal{C}} : r = [(r_0^2 - 3hp_{r0})^2 / r_0]^{1/3},$$

$$p_r = p_{r0} [(r_0^2 - 3hp_{r0})^2 / r_0^2]^{1/3}; \quad (30)$$

$$e^{h\mathcal{D}} : \theta = \theta_0 + hp_{\theta 0} / r_0^2,$$

$$p_r = p_{r0} + hp_{\theta 0}^2 / r_0^3; \quad (31)$$

$$e^{h\mathcal{F}} : r = \sqrt{r_0^2 + 2hQ^2 p_{r0} / r_0},$$

$$p_r = \frac{p_{r0}}{r_0} \sqrt{r_0^2 + 2hQ^2 p_{r0} / r_0}. \quad (32)$$

It is clear that all the analytical solutions in Equations (23), (24) and (29)-(32) are explicit functions of proper time τ or step size h . Although the compositions $H_2 + H_3$, $H_2 + H_3 + H_4$ and $H_2 + H_3 + H_4 + H_5$ can be solved analytically, their solutions are not expressed in terms of explicit functions of τ . The present splitting form (14) of the Hamiltonian H is one possible choice to satisfy the need.

The solutions of the Hamiltonian (7) over the time step h can be obtained approximately by a second order explicit symplectic integrator, namely, symmetric products of these exponential operators

$$S_2^H(h) = e^{\frac{h}{2}\mathcal{F}} e^{\frac{h}{2}\mathcal{D}} e^{\frac{h}{2}\mathcal{C}} e^{\frac{h}{2}\mathcal{B}} e^{h\mathcal{A}} \otimes e^{\frac{h}{2}\mathcal{B}} e^{\frac{h}{2}\mathcal{C}} e^{\frac{h}{2}\mathcal{D}} e^{\frac{h}{2}\mathcal{F}}. \quad (33)$$

It can compose a fourth-order symplectic scheme of Yoshida (1990)

$$S_4^H(h) = S_2^H(\gamma h) \circ S_2^H(\delta h) \circ S_2^H(\gamma h), \quad (34)$$

where $\delta = 1 - 2\gamma$ and $\gamma = 1/(2 - \sqrt[3]{2})$.

The two explicit symplectic algorithms for H are also suitable for K . The only one difference is H_1 replaced with

$$K_1 = \frac{1}{2r^2 \sin^2 \theta} (L - \frac{1}{2}\beta r^2 \sin^2 \theta)^2 - \frac{1}{2} (1 - \frac{2}{r} + \frac{Q^2}{r^2})^{-1} (E - \frac{Q^*}{r})^2. \quad (35)$$

Then, we obtain two explicit symplectic methods S_2^K and S_4^K for the Hamiltonian K .

4. Numerical simulations

At first, let us check the numerical performance of the proposed explicit symplectic integration algorithms for solving the system (10). Then, one of the new methods is selected to explore the orbital dynamics of charged massless particles in the system.

4.1. Evaluations of the new algorithms

In the previous work (Wang et al. 2021), the established explicit symplectic integrators for the Schwarzschild black hole surrounded by an external magnetic field were compared with a

conventional fourth-order Runge-Kutta integrator, second- and fourth-order explicit and implicit mixed symplectic algorithms (Mei et al. 2013b) and second- and fourth-order extended phase-space explicit symplectic-like methods (Luo et al. 2017). It was shown that the Runge-Kutta method has a secular drift in Hamiltonian errors and performs the poorest performance. The other algorithms at same order can exhibit good long-term stable error behavior for appropriate time steps and have no explicit differences among their Hamiltonian errors. Therefore, only the newly proposed explicit symplectic integrators in the present paper are considered to work out the Hamiltonian K .

Taking proper time step $h = 1$, we consider the parameters to be $E = 0.995$, $L = 4.6$, $\beta = 6.4 \times 10^{-4}$, $Q = 0.1$ and $Q^* = 10^{-4}$. The new second-order explicit symplectic integrator S2 (or the new fourth-order method S4) is used to integrate an orbit with initial conditions $r = 25$, $p_r = 0$ and $\theta = \pi/2$. The starting value of $p_\theta > 0$ is determined by Equation (13). In Figure 1(a), Hamiltonian errors $\Delta K = -1/2 - K$ in Equation (13) can remain bounded in an order of $\mathcal{O}(10^{-6})$ for S2 when the number of integration steps is 10^8 . S4 gives a higher accuracy with an order of $\mathcal{O}(10^{-9})$, but its errors grow linearly with time due to roundoff errors. Here are some analysis to these results. The test orbit has an approximate average period $T \approx 5000$. Truncation Hamiltonian error is $(h/T)^2 \sim 10^{-8}$ for S2 and $(h/T)^4 \sim 10^{-16}$ for S4. In fact, the error outputted at the end of the first step is 1.98×10^{-15} for S4. In addition, the machine yields a roundoff error in per computation, e.g. $\epsilon = 10^{-16}$ in a double-precision level. The roundoff errors grow in a rough estimation $n\epsilon$, where n is a number of computations. The roundoff errors are more important than the truncation errors when n is large enough. In an integration time $t = 200$, the Hamiltonian errors for S4 fast grow to 9×10^{-12} . When t spans this time and is less than 10^7 , the errors much slowly grow and basically remain stable at an order of $\mathcal{O}(10^{-9})$. With the integration continuing, the boundness of the Hamiltonian errors is destroyed by the roundoff errors. If the step size gets larger, e.g. $h=10$, the Hamiltonian errors are stabilized at an order of $\mathcal{O}(10^{-6})$. For $h=4$, the Hamiltonian errors remain bounded in an order of $\mathcal{O}(10^{-8})$.

Table 1: Performance of algorithms S2 and S4 with different time steps h . In the brackets, e.g., $(10^{-8}, \text{U}, 11'40'')$, 10^{-8} denotes the order of Hamiltonian error, U (or B) indicates the unboundedness (or boundedness) of Hamiltonian error, and $11'40''$ corresponds to CPU time (minute ', second "). The integration time reaches $\tau = 10^8$ for each step size.

h	0.1	1	4	10
S2	$(10^{-8}, \text{U}, 11'40'')$	$(10^{-6}, \text{B}, 1'12'')$	$(10^{-5}, \text{B}, 20'')$	$(10^{-4}, \text{B}, 7'')$
S4	no tested	$(10^{-9}, \text{U}, 3'34'')$	$(10^{-8}, \text{B}, 56'')$	$(10^{-6}, \text{B}, 23'')$

These results roughly indicate that a symplectic integrator can stabilize the Hamiltonian errors at the values larger than $\mathcal{O}(10^{-8})$ for 10^8 integration steps, which yield roundoff errors in the order of $\mathcal{O}(10^{-8})$. When the time step is $h = 1$ and the number of integration steps is 10^8 , the main error source for S2 is the truncation errors and therefore the Hamiltonian errors can remain stable at the order of $\mathcal{O}(10^{-6})$. However, the roundoff errors for S2 with time step $h = 0.1$ reach an order of $\mathcal{O}(10^{-7})$ after 10^9 integration steps. This forces the Hamiltonian errors with an order of $\mathcal{O}(10^{-8})$ to grow linearly. To clearly show the dependence of the magnitude and boundness of Hamiltonian errors and computational efficiency for algorithms S2 and S4 on the time step h , we give Table 1. Obviously, S2 with $h = 1$ or S4 with $h = 4$ is an optimal choice in the present cases.

The test orbit in Figure 1(a) is Orbit 1 colored red in Figure 1(b). Because this orbit is a single Kolmogorov-Arnold-Moser (KAM) torus on the Poincaré section, it is a regular quasi-periodic orbit. Black Orbit 2 with the initial value $r = 90$, consisting of 11 small islands, is also a regular many-islands KAM torus. The occurrence of resonance and chaos will become easy for such an orbit with many islands. However, blue Orbit 3 with the initial value $r = 50$ has many discrete points distributed in a small area on the Poincaré section. This kind of phase space structure indicates the chaoticity of Orbit 3. The purple orbit with the initial value $r = 110$ is also chaotic. In spite of the onset of chaos, the possibility of “islands of regularity” like Orbits 1 and 2 is still existent. Based on KAM theorem, the minima of the effective potential in the equatorial plane correspond to stable circular orbits, which are related to regular harmonic oscillatory motions for the description of Keplerian accretion disks of stellar mass black holes. Moreover, all trajectories that are bounded in the vicinity of the equatorial

plane are also regular (Kološ et al. 2015). These regular motions can successfully explain the quasi-periodic oscillations of X-ray flux from several microquasars (Kološ et al. 2017; Tursunov & Kološ 2018). There is another island of regularity related to the motion along the magnetic field lines (Tursunov et al. 2020a). In some cases, a hot spot can exhibit quasi-circular motion along a single orbit (Tursunov et al. 2020b). However, the quasicircular motion may become chaotic because the axial symmetry of the system is broken so that the hot spot’s angular momentum is not conserved. The absence of the angular momentum is caused by the inclination angle of the hot-spot orbit from the equatorial plane or of the magnetic field lines with respect to the black hole’s spin axis.

If regular single-island Orbit 1 is replaced with regular many-islands Orbit 2 or chaotic Orbit 3, the numerical performance of the two algorithms S2 and S4 has no explicit differences. In other words, no dynamical behavior of orbits but a step size mainly affects the quality of the proposed algorithms. In the later discussions, we employ S4 with the appropriate time step $h = 4$ to investigate the related dynamical features of the Hamiltonian K when charge parameters Q and Q^* , and magnetic parameter β are varied.

4.2. Applications

To show the dependence of the orbital dynamics of order and chaos on the black hole’s charge Q or the Coulomb parameter Q^* , we fix the parameters E , L and β in Figure 1. Of course, different values of Q and Q^* are adopted.

In fact, the phase-space structures for the case of $Q = Q^* = 0$ are similar to those for the case of $Q = 0.1$ and $Q^* = 10^{-4}$ in Figure 1(b). To clearly show how the orbital dynamics of order and chaos depends on the charge Q , we consider the choice of $Q \gg Q^*$. Fixing $Q^* = 10^{-4}$, we give Q differ-

ent larger values. The result for $Q = 0.1$ is also suitable for the case of $Q = 0.3$. However, the phase-space structures for $Q = 0.6$ in Figure 2(a) are somewhat different from those for $Q = 0.1$. Orbit 2 is ordered in Figure 1(b), but becomes chaotic in Figure 2(a). Orbit 3 that is chaotic in Figure 1(b) is a regular orbit with many loops in Figure 2(a). Compared with those for the case of $Q = 0.6$ in Figure 2(a), the orbits exist some differences for the case of $Q = 0.8$ in Figure 2(b). The blue islands in Figure 2(a) become an ordered single torus in Figure 2(b). The green ordered single torus in Figure 2(a) is weakly chaotic in Figure 2(b). When $Q = 1$, the extent of chaos in Figure 2(c) is not typically strengthened. A result seems to be concluded from Figures 1(b) and 2(a)-2(c). An increase of the black hole's charge Q may exert some influence on the phase-space structures, but does not bring an apparent dynamical transition from order to chaos. Namely, it is not considerably sensitive to alter the dynamical orbital properties. It does not typically enhance the extent of chaos, either.

What about the dynamical transition with an increase of the Coulomb parameter Q^* for a given smaller value (e.g., $Q = 10^{-4}$)? Figures 2(d) and 2(e) describe that the chaotic behavior existing in the case of $Q = Q^* = 0$ gradually dies out when Q^* increases, such as $Q^* = 0.1$ and 0.3 . As Q runs from a smaller value $Q = 10^{-4}$ to a larger value $Q = 0.3$, the phase-space structures have no dramatic differences between Figures 2(f) and 2(e). In fact, the phase-space structures for the case of $Q = Q^* = 0.1$ are basically similar to those for the case of $Q = 10^{-4}$ and $Q^* = 0.1$ in Figure 2(d). The orbits for the case of $Q = 0.1$ and $Q^* = 0.3$ are also the same as those for the case of $Q = 10^{-4}$ and $Q^* = 0.3$ in Figure 2(e). This result shows again that no Q but Q^* mainly affects the regular and angular dynamics of orbits. In particular, a positive value of Q^* weakens the strength of chaos. On the other hand, a negative value of Q^* can easily induce the occurrence of chaos, and the extent of chaos is drastically strengthened when the magnitude of negative Coulomb parameter Q^* increases, as shown in Figures 2(g)-2(i). Notice that the orbits between the case of $Q = 0.1$ and $Q^* = -0.1$ and the case of $Q = 10^{-4}$ and $Q^* = -0.1$ in Figure 2(g) are almost the same. So are the orbits between the case of $Q = 0.1$ and $Q^* = -0.3$ and

the case of $Q = 10^{-4}$ and $Q^* = -0.3$ in Figure 2(i). When Coulomb parameter Q^* is negative, the Coulomb part of the electromagnetic potential A_t in Equation (9) is positive.

What will happen if magnetic parameter β increases but parameters E, L, Q and Q^* are fixed? Red Orbit 1 with parameters $Q = 0.1$ and $Q^* = 10^{-4}$ in Figure 1(b) is tested. The orbit is twisted for $\beta = 9.7 \times 10^{-4}$ in Figure 3(a), becomes a three-islands orbit for $\beta = 9.9 \times 10^{-4}$ in Figure 3(b), and is finally evolved to a strong chaotic orbit for $\beta = 1.1 \times 10^{-3}$ in Figure 3(c). Given $Q = 10^{-4}$ and $Q^* = 0.1$, the orbit becomes many-islands, weakly chaotic and strong chaotic orbits as β increases from 9.7×10^{-4} to 1.1×10^{-3} in Figures 3(d)-3(f). For $Q = Q^* = 0.1$, the orbit is evolved to a twisted single torus, a many-islands orbit and a strong chaotic orbit with an increase of β in Figures 3(g)-3(i). Particular for $Q^* = -0.1, -0.3$ and $\beta = 9.7 \times 10^{-4}, 9.9 \times 10^{-4}, 1.1 \times 10^{-3}$, strong chaos (not plotted) always occurs. All the results prove that an increase of magnetic parameter β gives rise to enhancing the chaotic effect.

Why do the two charge parameters Q and Q^* have completely different effects on the dynamical behavior of orbits? Why does an increase of negative parameter Q^* or magnetic parameter β lead to strengthening the extent of chaos? To answer these questions, we expand the term $(\)^{-1}$ in Equation (35) and rewrite Equation (35) as follows:

$$\begin{aligned}
K_1 \approx & -\frac{1}{2}(\beta L + E^2) + \frac{\beta^2}{8}r^2 \sin^2 \theta - \frac{E^2}{r} \\
& + \frac{EQ^*}{r} + \frac{L^2}{2r^2 \sin^2 \theta} + \frac{Q^2 E^2}{2r^2} \\
& + \frac{Q^*}{2r^2}(4E - Q^*) + \dots \quad (36)
\end{aligned}$$

The second term $V_1 = \beta^2 r^2 \sin^2 \theta / 8$ in Equation (36) is a magnetic field force acting as a gravitational effect to the particle. The third term $V_2 = -E^2/r$ is the gravity of the black hole to the particle. The Coulomb term $V_3 = EQ^*/r$ acts as a repulsive force effect to the particle for $Q^* > 0$, but a gravitational force effect for $Q^* < 0$. The fifth term $V_4 = L^2/(2r^2 \sin^2 \theta)$ is an inertial centrifugal force caused by the particle's angular momentum L . The sixth term $V_5 = Q^2 E^2/(2r^2)$ is an electric field force, which acts as a repulsive force effect to the particle. The magnetic field part V_1 is a fundamental source for causing the nonintegrability

and chaoticity of the system (10). For $\beta = 0$, the system (10) is integrable and nonchaotic. When β is extremely small in the case of $Q = 0$ corresponding to $V_3 = V_5 = 0$, the black hole's gravity V_2 is a dominant force and therefore chaos does not possibly occur, either. With β increasing, the magnetic field force increases. Only when V_1 appropriately matches with V_2 , may chaos occur. The extent of chaos can be strengthened with an increase of the magnetic parameter from the global phase-space structure. As to V_3 and V_5 to the contributions of particle's dynamics, $V_3 \sim 1/r$ is a primary part, and $V_5 \sim 1/r^2$ is a secondary part for $r \gg 2$ and $|Q| \leq 1$. This can explain why the variation of Q^* rather than the variation of Q is considerably sensitive to affect the regular and chaotic dynamics of particles' orbits. For $Q^* > 0$, the Coulomb term, as a repulsive force, reduces the gravitational effect from the magnetic field. On the contrary, the Coulomb term, as a gravitational force, enhances the magnetic field gravitational force effect. Thus, an increase of the magnitude of negative Coulomb parameter Q^* leads to strengthening the extent of chaos, whereas an increase of positive Coulomb parameter Q^* does not.

5. Conclusions

In this paper, we are devoted to designing explicit symplectic integrators for a Hamiltonian system of charged test particles moving around the Reissner-Nordström black hole immersed into an external magnetic field. In our construction, the Hamiltonian is separated into five independently integrable parts with analytical solutions as explicit functions of proper time. These analytical solutions are used to yield second- and fourth-order explicit symplectic integrators in symmetric combinations.

The proposed algorithms are shown to exhibit good long term numerical performance in the Hamiltonian conservation, numerical accuracy and computational efficiency. Such good numerical performance does not mainly depend on the regular and chaotic dynamical behavior of orbits but a step size. Thus, an optimal step size is necessary.

The fourth-order explicit symplectic integrator with an optimal step size is applied to well explore the dynamics of charged particles around

the Reissner-Nordström black hole with an external magnetic field. We focus on the influences of the black hole's charge, the Coulomb part of the electromagnetic potential and the magnetic parameter on the dynamical behavior. The magnetic parameter plays an important role in causing the nonintegrability and chaoticity of the system. Under some circumstances, the extent of chaos is strengthened from the global phase-space structure as the magnetic parameter increases. No the variation of the black hole's charge but the variation of the Coulomb part is considerably sensitive to affect the regular and chaotic dynamics of particles' orbits. A positive Coulomb part is easier to induce chaos than a negative one.

Acknowledgments

The authors are very grateful to a referee for useful suggestions. This research has been supported by the National Natural Science Foundation of China [Grant Nos. 11533004, 11973020 (C0035736), 11803020, 41807437, U2031145] and the Natural Science Foundation of Guangxi (Grant Nos. 2018GXNSFGA281007 and 2019JJJD110006).

REFERENCES

- Abbott, B. P., Abbott, R., Abbott, T. D., et al. 2016, *Phy. Rev. Lett.*, 116, 061102
- Bacchini, F., Ripperda, B., Chen, A. Y., Sironi, L. 2018a, *Astropys. J. Suppl.*, 237, 6
- Bacchini, F., Ripperda, B., Chen, A. Y., Sironi, L. 2018b, *Astropys. J. Suppl.*, 240, 40
- Brown, J. D. 2006, *Phys. Rev. D*, 73, 024001
- Carter, B. 1968, *Phy. Rev.*, 174, 1559
- Deng, C., Wu, X., & Liang, E. 2020, *MNRAS*, 496, 2946
- EHT Collaboration, et al. 2019a, *ApJL*, 875, L1 (Paper I)
- EHT Collaboration et al. 2019b, *ApJL*, 875, L4 (Paper IV)
- EHT Collaboration et al. 2019c, *ApJL*, 875, L6 (Paper VI)
- Felice, D. d, & Sorge, F. 2003, *Class. Quantum Grav.*, 20, 469

- Feng, K. 1986, *Journal of Computational Mathematics*, 44, 279
- Hairer, E., Lubich, C. & Wanner, G. 1999, *Geometric Numerical Integration*, Springer-Verlag, Berlin
- Hu, S., Wu, X., Huang, G., & Liang, E. 2019, *ApJ*, 887, 191
- Kerr, R. P. 1963, *Phys. Rev. Lett.*, 11, 237
- Kološ, M., Stuchlík, Z., & Tursunov, A. 2015, *Class. Quantum Grav.*, 32, 165009
- Kološ, M., Tursunov, A., & Stuchlík, Z. 2017, *Eur. Phys. J. C*, 77, 860
- Kopáček, O., Karas, V., Kovář, J., & Stuchlík, Z. 2010, *ApJ*, 722, 1240
- Kopáček, O., & Karas, V. 2014, *ApJ*, 787, 117
- Li, D., & Wu, X. 2017, *Mon. Not. R. Astron. Soc.*, 469, 3031
- Li, D., & Wu, X. 2019, *Eur. Phys. J. Plus*, 134, 96
- Liao, X. H. 1997, *Celest. Mech. Dyn. Astron.*, 66, 243
- Lichtenberg, A. J., & Lieberman, M. A. 1983, *Regular and Chaotic Dynamics* (Springer-Verlag, New York)
- Liu, L., Wu, X., Huang, G. Q., & Liu, F. 2016, *Mon. Not. R. Astron. Soc.*, 459, 1968
- Lubich, C., Walther, B., & Brüggemann, B. 2010, *Phys. Rev. D*, 81, 104025
- Luo, J., Wu, X., Huang, G., & Liu, F. 2017, *ApJ*, 834, 64
- Mei, L., Ju, M., Wu, X., & Liu, S. 2013a, *Mon. Not. R. Astron. Soc.*, 435, 2246
- Mei, L., Wu, X., & Liu, F. 2013b, *Eur. Phys. J. C*, 73, 2413
- Pánis, R., Kološ, M., Stuchlík, Z. 2019, *Eur. Phys. J. C*, 79, 479
- Pihajoki, P. 2015, *Celest. Mech. Dyn. Astron.*, 121, 211
- Preto, M., & Saha, P. 2009, *ApJ*, 703, 1743
- Reissner, H. 1916, *Ann. Phys.*, 50, 106
- Ruth, R. D. 1983, *IEEE Trans. Nucl. Sci. NS* 30, 2669-2671
- Seyrich, J., & Lukes-Gerakopoulos, G. 2012, *Phys. Rev. D*, 86, 124013
- Schwarzschild, K. 1916, *Stizber. Deut. Akad. Wiss., Berlin, K1. Math.-Phys. Tech. s.*, 189
- Stuchlík, Z., & Kološ, M. 2016, *Eur. Phys. J. C*, 76, 32
- Stuchlík, Z., Kološ, M., Kovář, J., & Tursunov, A. 2020, *Universe*, 6, 26
- Swope, W. C., Andersen, H. C., Berens, P. H., & Wilson, K. R. 1982, *J.Chem. Phys.* 76, 637
- Takahashi, M., & Koyama, H. 2009, *ApJ*, 693, 472
- Tsang, D., Galley, C. R., Stein, L. C., & Turner, A. 2015, *ApJL*, 809, L9
- Tursunov, A. A., & Kološ, M. 2018, *Physics of Atomic Nuclei*, 81, 279
- Tursunov, A., Stuchlík, Z., Kološ, M., Dadhich, N., & Ahmedov, B. 2020a, *ApJ*, 895, 14
- Tursunov, A., Zajaček, M., Eckart, A., Britzen, S., & Stuchlík, Z. 2020b, *ApJ*, 897, 99
- Wang Y., Sun W., Liu F., Wu X. 2021, *ApJ* (Paper I), 907, 66
- Wisdom, J., & Holman, M. 1991, *AJ*, 102, 1528
- Yi, M., & Wu, X. 2020, *Phys. Scr.*, 95, 085008
- Yoshida, H. 1990, *Phys. Lett. A*, 150, 262
- Zhong, S. Y., Wu, X., Liu, S. Q., & Deng, X. F. 2010, *Phys. Rev. D*, 82, 124040

This 2-column preprint was prepared with the AAS L^AT_EX macros v5.2.

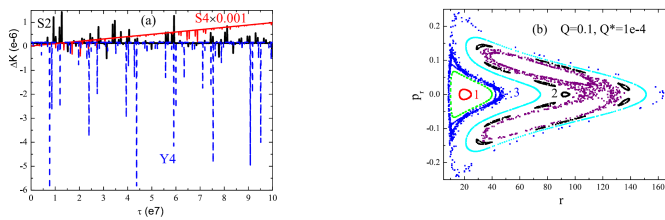


Fig. 1.— (a) Hamiltonian errors $\Delta K = -1/2 - K$ in Equation (13) for the proposed algorithms solving the system (10). The parameters are $E = 0.995$, $L = 4.6$, $\beta = 6.4 \times 10^{-4}$, $Q = 0.1$ and $Q^* = 1 \times 10^{-4}$. A test orbit has initial conditions $r = 25$, $p_r = 0$ and $\theta = \pi/2$. The starting value of $p_\theta > 0$ is determined by Equation (13). The new second-order and fourth-order explicit symplectic integrators S2 and S4 take proper time step $h = 1$. The realistic errors for S4 are 1000 times smaller than the plotted errors. The errors for S2 remain bounded and stable in an order of $\mathcal{O}(10^{-6})$, whereas do not for S4 due to roundoff errors. However, such a secular drift in Hamiltonian errors is missing when large proper time step $h = 10$ is used in the fourth-order method Y4. These facts show that the new algorithms with appropriate time steps can share good properties of a standard symplectic integrator in long-term stabilized error behavior. (b) Poincaré sections on the plane $\theta = \pi/2$ and $p_\theta > 0$, given by algorithm S2 with proper time step $h = 1$. The test orbit in panel (a) is regular Orbit 1 colored red in panel (b).

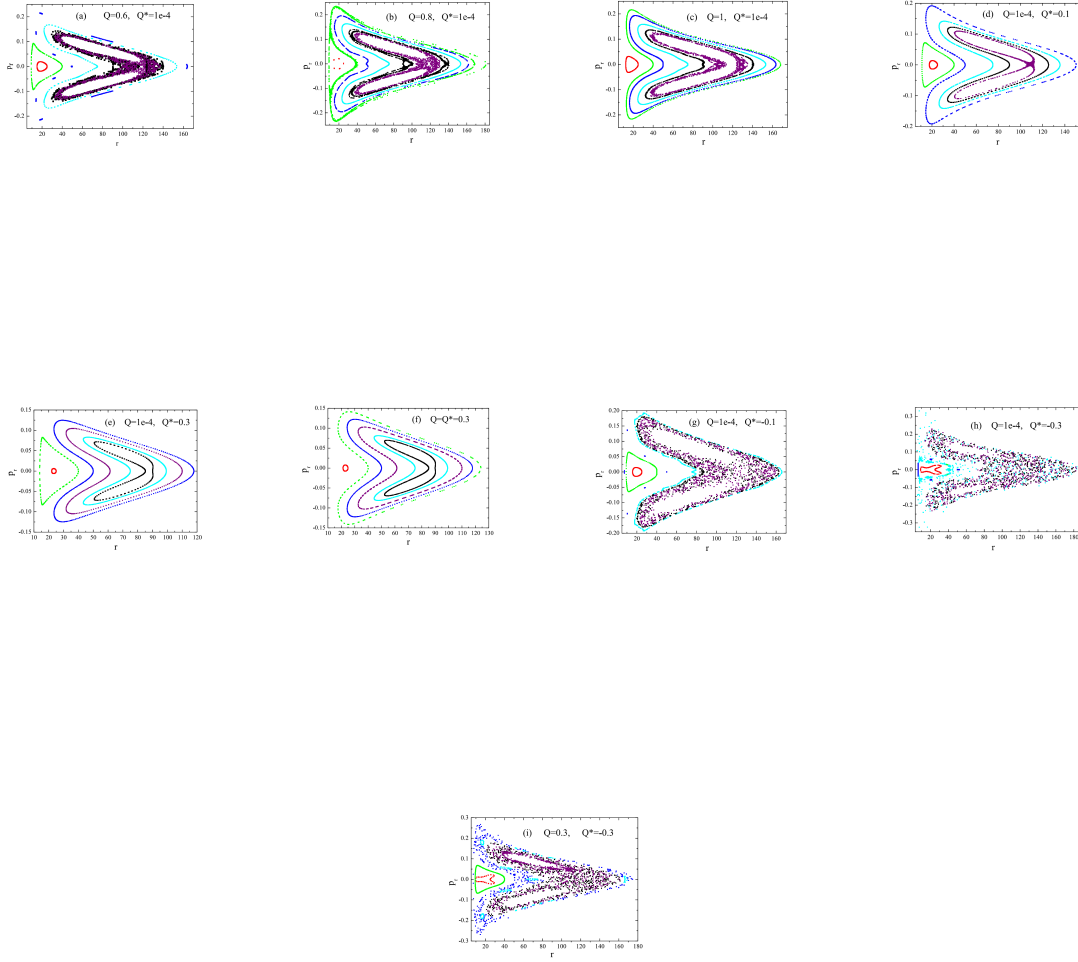


Fig. 2.— Same as Figure 1(b), but different values of parameters Q and Q^* are given.

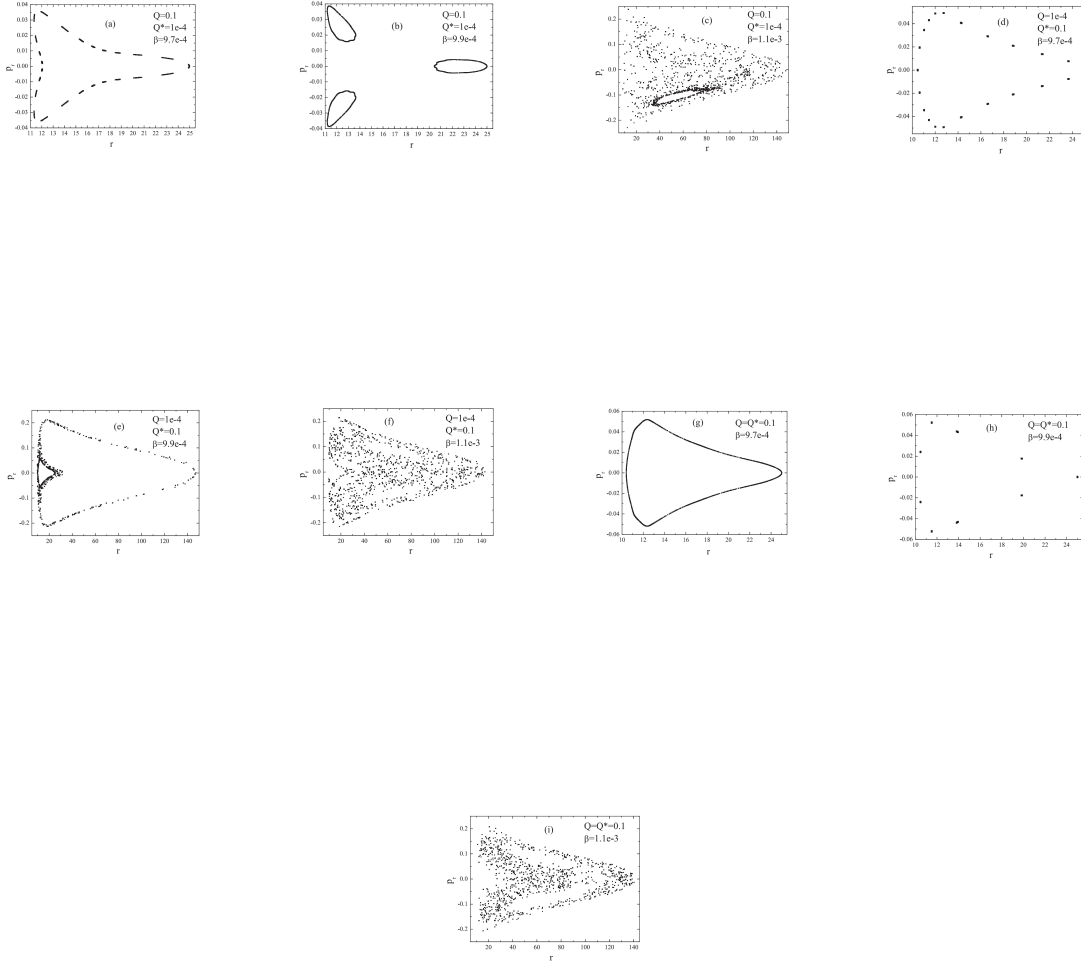


Fig. 3.— Same as Orbit 1 colored red in Figure 1(b), but different combinations of parameters Q , Q^* and β are given.